

The most significant aspect of the fragmentation process discussed here is the possibility of distinguishing leucine from isoleucine in peptides that give rise to C-terminal ions. This complements the similar significance of the  $a_n$  ion types,  $a_n-42$  for Leu and  $a_n-28$  for Ile, observed for peptides that favor retention of the charge on N-terminal fragments (6). Earlier efforts to differentiate leucine from isoleucine by mass spectrometry had met with only limited success (3). Of secondary importance is the confirmatory aspect of the presence or absence of a  $w_n$  ion corresponding to amino acids at the N-terminal positions of these ions, indicating the presence or absence of amino acids that possess a readily cleaved  $\beta,\gamma$  bond. Finally the  $m/z$  value of  $w_n$  ions allow the confirmation of the position of amino acids substituted at the  $\beta$  carbon, such as threonine or valine. A note of caution should be added, however, because the fragmentation of a  $\beta,\gamma$  bond of a side chain of an amino acid next to that representing the N-terminus of the fragment may occur.

#### ACKNOWLEDGMENT

The authors are indebted to H. A. Scoble (MIT) for his useful comments.

**Registry No.** 1, 110143-90-3; 2, 110143-91-4; 3, 110143-92-5; 4, 87620-09-5; 5, 83404-43-7; 6, 110143-93-6; 7, 110143-94-7; 8, 110143-95-8; 9, 62526-81-2; 11, 110143-96-9; 12, 80501-44-6; 13, 58-82-2; 14, 15958-92-6; 15, 16875-11-9; 16, 110143-97-0; 17, 110143-98-1; 18, 71901-21-8; 19, 110143-99-2; 20, 110144-00-8; 21, 110144-01-9; 22, 75645-19-1; 23, 110144-02-0; 24, 110144-03-1; 25,

53749-61-4; 26, 33507-63-0; 27, 71977-09-8; 28, 110144-04-2; 29, 110144-05-3; 30, 59004-96-5; 31, 25422-31-5; 32, 10047-33-3; 33, 4419-81-2; leucine, 61-90-5; isoleucine, 73-32-5.

#### LITERATURE CITED

- (1) Barber, M.; Bordoli, R. S.; Sedgwick, R. D.; Tyler, A. N. *J. Chem. Soc., Chem. Commun.* **1981**, 325-327.
- (2) Martin, S. A.; Biemann, K. *Int. J. Mass Spectrom. Ion Processes* **1987**, *78*, 213-228.
- (3) Martin, S. A.; Biemann, K. *Mass Spectrom. Rev.* **1987**, *6*, 1-76.
- (4) Roepstorff, P.; Fohlman, J. *Biomed. Mass Spectrom.* **1984**, *11*, 601.
- (5) Sato, K.; Asada, T.; Ishihara, M.; Kunihiro, F.; Kammei, Y.; Kubota, E.; Costello, C. E.; Martin, S. A.; Scoble, H. A.; Biemann, K. *Anal. Chem.* **1987**, *59*, 1652-1659.
- (6) Martin, S. A.; Biemann, K. Presented at the 34th Annual Conference on Mass Spectrometry and Allied Topics, Cincinnati, OH, 1986.
- (7) Martin, S. A., unpublished results.
- (8) Biemann, K.; Martin, S. A.; Scoble, H. A.; Johnson, R. S.; Papayannopoulos, I. A.; Biller, J. E.; Costello, C. E. In *Mass Spectrometry in the Analysis of Large Molecules*; McNeal, C. J., Ed.; Wiley: Sussex, England, 1986; pp 131-149.
- (9) Hoog, J.-O.; Von Bahr-Lindstrom, H.; Josephson, S.; Wallace, B. J.; Kushner, S. R.; Jornvall, H.; Holmgren, A. *Biosci. Rep.* **1984**, *4*, 917-923.
- (10) Gleason, F. K.; Whittaker, M. M.; Holmgren, A.; Jornvall, H. *J. Biol. Chem.* **1985**, *260*, 9567-9573.
- (11) Williams, D. H.; Bradley, C. V.; Santikarn, S.; Bojesen, G. *Biochem. J.* **1981**, *201*, 105-117.
- (12) Jensen, N. J.; Tomer, K. B.; Gross, M. L. *J. Am. Chem. Soc.* **1985**, *107*, 1863-1868.

RECEIVED for review May 14, 1987. Accepted July 20, 1987. This work was supported by research grants from the National Institutes of Health to K. Biemann (RR00317 and GM05472) and to J. T. Watson (RR00480).

## Preparation and Electrochemical Characterization of Ultramicroelectrode Ensembles

Reginald M. Penner<sup>1</sup> and Charles R. Martin\*

Department of Chemistry, Texas A&M University, College Station, Texas 77843

**A new procedure for preparing ultramicrodisk electrode ensembles is described. This procedure is based on electrochemical deposition of platinum into the pores of a microporous polycarbonate host membrane. This procedure is simple and fast and requires only conventional, inexpensive electrochemical instrumentation. Furthermore, this new procedure can be used to prepare ensembles with very small and uniform element radii. We have used this procedure to prepare ultramicrodisk ensembles with elements having radii as small as 1000 Å. These are the smallest element radii reported in the literature to date. Electrochemical methods were used to characterize the ensembles prepared using this new procedure. These studies show that the new ensembles yield electrochemical responses that are consistent with established theory.**

Theoretical analyses suggest that ultramicroelectrode arrays (UMA's) may have a number of important advantages over conventional, macro-sized electrodes (1-4). For example, digital simulations suggest that cyclic voltammetric experi-

ments at UMA's containing disk-shaped elements can be used to measure heterogeneous rate constants that are too large for measurement via cyclic voltammetry at macro-sized electrodes (1). As the size of the microdisks in the UMA decreases, the magnitude of the rate constant which can be reliably measured increases (1).

UMA's can also show higher signal-to-noise ratios (and thus lower detection limits in electroanalytical experiments) than conventional, macro-sized electrodes (1, 2). This improvement in signal-to-noise ratio results because, under optimal conditions, the faradaic signal associated with electrolysis of the analyte is proportional to the total geometric area of the UMA (i.e., active plus inactive area) whereas the noise is proportional to only the active element area (see below) (1-3). Equations developed by Pons et al. show that for chronoamperometric experiments at UMA's with disk-shaped elements, the enhancement in sensitivity, relative to the macro-sized electrode, increases as the diameter of the elements decreases (2).

The above discussion suggests that if electrochemists are to reap maximal benefits from UMA's with disk-shaped elements, the microdisks should be made as small as possible. Osteryoung et al. have recently used microlithographic techniques to prepare UMA's composed of 0.375- $\mu$ m-radii disks (4). The microdisks in these arrays are the smallest to be reported in the literature to date. Although electron beam and X-ray microlithography possess sufficient resolution to

<sup>1</sup> Present address: Department of Chemistry, Stanford University, Stanford, CA 94305.

Table I. Nuclepore Membrane Specifications

pore radius, <sup>a</sup> μm	pore density, <sup>a</sup> pores cm <sup>-2</sup>	fractional pore area <sup>b</sup>	thickness, <sup>a</sup> μm	average distance between pores, <sup>c</sup> μm
0.5	2 × 10 <sup>7</sup>	0.157	10	5
0.1	3 × 10 <sup>8</sup>	0.094	10	1

<sup>a</sup> From Nuclepore, Inc., product literature. Nominal precision of pore diameter is +0% to -20%. Nominal precision of pore density is ±15% (8). <sup>b</sup> Surface area of pores divided by total surface area of membrane. Since the pores become the UME elements, this fraction is the active electrode area divided by the total geometric area. <sup>c</sup> Average distances are estimated from scanning electron micrographs of as-received Nuclepore membranes.

allow microdisk arrays of smaller elements to be prepared (4), these methods require instrumentation and expertise not usually found in the electrochemical or analytical laboratory (5-7).

We have developed a new procedure for constructing ensembles of ultramicrodisk electrodes. The term ensemble rather than array is used because the elements in these devices are not evenly spaced. This procedure is simple and quick and requires only routine, inexpensive electrochemical instrumentation. Furthermore, this procedure can be used to prepare ensembles with very small and uniform element radii. In principle, element radii as small as 50 Å are possible using this approach; the ensembles described in this paper have elements with radii of 1000 and 5000 Å.

We describe this new procedure and present results of voltammetric investigations of the resulting ultramicroelectrode ensembles (UME's) in this publication. Two types of voltammetric experiments were conducted. The first involved measurement of capacitive currents at the UME's so as to obtain information about the exposed element surface area. The second set of experiments involved measurement of faradaic currents and were conducted to determine whether the UME's function according to established electrochemical theory (1-4).

## EXPERIMENTAL SECTION

**Chemicals and Equipment.** Chloroplatinic acid (99.995%, Aldrich), Fischer reagent grade H<sub>2</sub>SO<sub>4</sub>, and Southwestern Analytical Chemicals electrometric grade Bu<sub>4</sub>NClO<sub>4</sub> were used as received. Milli Q 18-MΩ water was used for rinsing and for all aqueous solutions. Solutions with acetonitrile were prepared from Burdick and Jackson Spectrograde acetonitrile. Nuclepore 1.0 and 0.2 μm pore diameter polycarbonate membranes were generously donated by Nuclepore Corp. The specifications of these membranes are listed in Table I (8).

A hot polyethylene solution was used in the preparation of the ultramicroelectrode ensembles (see next section). This solution was prepared by melting 1000 molecular weight polyethylene (Polysciences Inc., no. 7662) at 120 °C and then dissolving into this melt a low density, high molecular weight, polyethylene (Polysciences Inc., no. 3123). A 5% solution was prepared.

Platinum deposition was accomplished with a Bioanalytical Systems Model CV-27 potentiostat. Electrochemical measurements were made with a PAR Model 173 potentiostat in conjunction with a PAR Model 175 programmer and a Houston Instruments Model 2000 XY recorder or a Nicolet Model 206 digital storage oscilloscope. Ninety percent *iR* compensation was employed for all measurements (9). All solutions were purged with nitrogen prior to use. Scanning electron micrographs were obtained on a JEOL JSM-25SII scanning electron microscope at an accelerating voltage of 25 kV.

**Procedure for Preparing Ultramicroelectrode Ensembles.** The procedure developed stems from our work with electronically conductive composite polymer membranes (10, 11). This procedure is summarized schematically in Figure 1 and discussed in detail in the following paragraphs. A porous host membrane

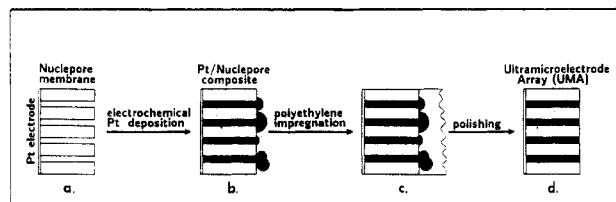


Figure 1. Schematic diagram of the procedure used to prepare ultramicrodisk electrode ensembles.

is immobilized onto the surface of a Pt-disk electrode (Figure 1a). This membrane-modified electrode is then immersed in a solution of chloroplatinic acid and Pt is deposited electrochemically in the pores of the host membrane. Electrochemical deposition is continued until the Pt layer begins to overgrow the surface of the host membrane (Figure 1b). The surface of the Pt/Nuclepore composite membrane is then impregnated with polyethylene (PE) by immersion in molten PE solution (see Figure 1c and discussion below). Finally, the PE and excess Pt are removed by polishing, revealing the UME (Figure 1d).

The key point in Figure 1 is that the pores of the host act as templates for the elements of the UME. The geometries and dimensions of the pores define the geometries and dimensions of the UME elements. Furthermore, the pore density defines the UME element density.

Nuclepore polycarbonate membranes were used as the host materials (8). These membranes are prepared by a patented irradiation/chemical etch technique and contain linear, cylindrical pores of nearly uniform pore diameter. This ensures that the elements of the UME are all circular and of approximately the same diameter. Furthermore, because membranes with pore radii ranging from 6 μm to 50 Å are available commercially, UME's with a broad range of element radii can, in principle, be prepared. In addition, these membranes have very high pore densities, ranging from approximately 1 × 10<sup>5</sup> pores cm<sup>-2</sup> for the 6.0 μm pore membranes to approximately 6 × 10<sup>8</sup> pores cm<sup>-2</sup> for the 50 Å pore membranes (7). Finally, polycarbonate has good chemical and thermal stability. For all of these reasons, Nuclepore is the ideal host material for preparing UME's.

Pt disks (*r* = 4 mm) were used as the substrate electrodes. Because prior studies showed that better substrate surface/membrane contact is achieved with convex substrate electrodes than with conventional planar electrodes (12), convex electrodes were used here. Convexity was introduced by polishing the circumference of the electrodes more than the center. Substrate electrodes were prepared and polished as described previously (10).

Nuclepore membrane of the desired pore diameter was wetted with acetonitrile, stretched over the convex electrode, and held in place with a sleeve of heat-shrinkable Teflon tubing (Figure 2). A conventional two-compartment electrochemical cell consisting of the membrane-modified working electrode, an aqueous saturated calomel electrode (SCE), and a Pt-flag counter electrode was used for Pt deposition. Aqueous 10<sup>-2</sup> M chloroplatinic acid, which was 0.5 M in H<sub>2</sub>SO<sub>4</sub>, served as the electrolysis solution.

Pt deposition was accomplished by repeatedly scanning the potential of the working electrode between 0.4 and -0.3 V (vs. SCE, scan rate 50 mV s<sup>-1</sup>). A typical cyclic voltammogram obtained during the deposition process is shown in Figure 3. Deposition was continued until the Nuclepore surface was overgrown with Pt. This proved necessary because electron micrographs showed that membranes that were not overgrown contained a fraction of pores that were either devoid of or only partially filled with Pt.

It is important to point out that prior to emergence of the Pt fibers from the pores of the Nuclepore membrane, the membrane surface is reflective and black. After emergence, this surface is no longer reflective and is dull gray in appearance. This change in the appearance of the surface of the Pt/Nuclepore composite membrane can be used to determine when sufficient Pt has been deposited. Deposition times of ca. 4 h were required for the UME's described here. After Pt impregnation, the composite membranes were extracted in Milli Q water for an hour to remove residual plating solution. Electrodes were then dried in vacuo for 4 h at 80 °C.

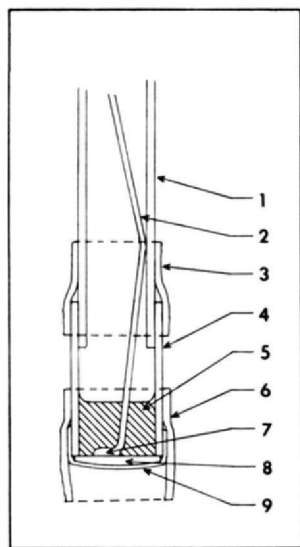


**Figure 2.** Schematic diagram of the Nuclepore membrane modified electrode used to prepare the ultramicroelectrode ensembles: 1, 6-mm glass tube; 2, Cu wire; 3, heat shrinkable Teflon tube; 4, 9-mm glass tube; 5, electron microscopy grade epoxy; 6, heat shrinkable Teflon tube; 7, solder contact; 8, convex Pt substrate; 9, Nuclepore/Pt composite UME.

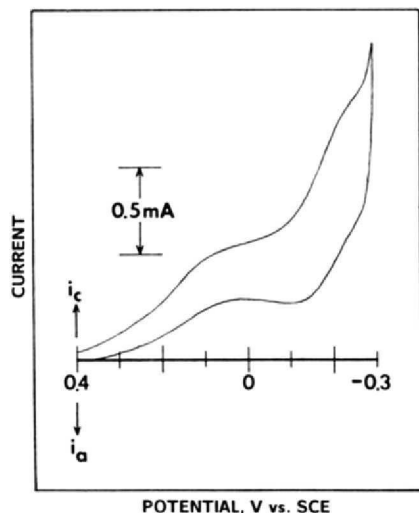


**Figure 3.** Initial cyclic voltammogram for Pt deposition at a 1.0  $\mu\text{m}$  pore diameter Nuclepore membrane modified electrode: scan rate 50 mV/s; 10 mM  $\text{H}_2\text{PtCl}_6$ , 0.2 M  $\text{H}_2\text{SO}_4$ .

In our initial attempts to prepare UME's using this approach, the electrodes were, at this point, polished to remove the excess Pt and examined electrochemically. These UME's showed capacitive currents, that were much higher than expected, suggesting that solution was creeping between the Pt and the host membrane. To circumvent this problem, the Pt-Nuclepore composite membrane electrodes were impregnated with low molecular weight PE before polishing. This drastically lowered the capacitive currents observed at the UME (see capacitance section below).

PE was incorporated by immersing the Pt/Nuclepore composite membrane electrodes in molten (120  $^\circ\text{C}$ ) PE solution in a vacuum oven; the membranes were exposed to the PE solution for 15 min. The electrodes were then allowed to stand at room temperature for ca. 2 h to allow the PE to harden. This treatment leaves a thick PE coating over the Pt-impregnated Nuclepore surface (Figure 1c). Immediately before use, the PE-covered surface was hand-polished with 0.05- $\mu\text{m}$  alumina. Complete removal of excess PE and Pt is signaled by a change in color of the electrode surface from light gray to black.

## RESULTS AND DISCUSSION

**Electron Microscopy.** A scanning electron micrograph of a typical UME is shown in Figure 4a. Clearly, Pt is de-

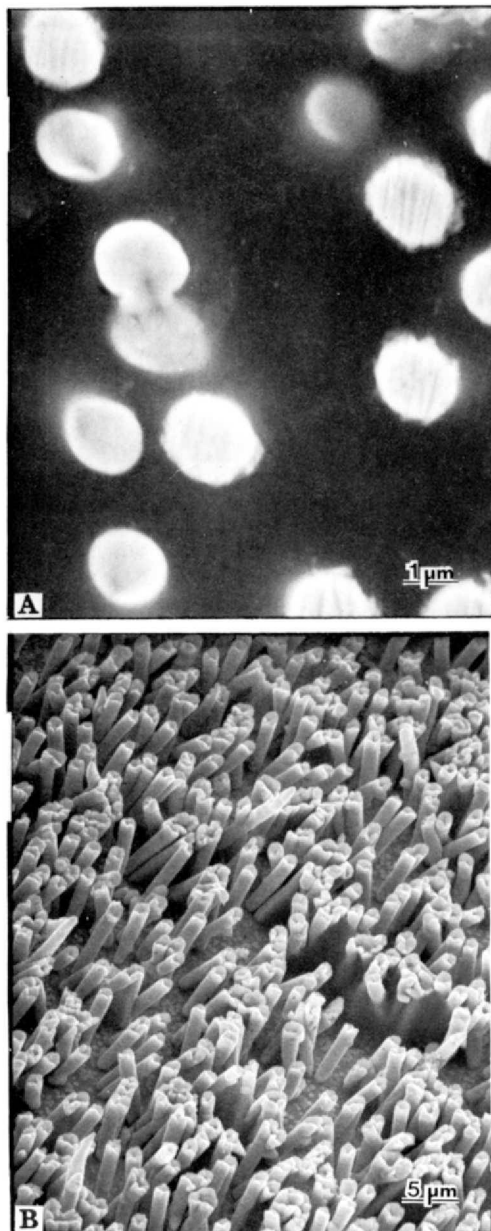


**Figure 4.** Electron micrographs of (A) the surface of an UME prepared from Nuclepore membrane with 1.0- $\mu\text{m}$ -diameter pores and of (B) Pt fibrils obtained after polycarbonate host membrane is dissolved away from the UME shown in part A.

posited only within the pores of the host. Furthermore the exposed Pt microdisks retain the size and near circular shape of the pores in the host membrane. Prior studies have shown that the Nuclepore host membrane is quite soluble in  $\text{CH}_2\text{Cl}_2$  (11). Dissolving away the host membrane affords an opportunity for observing the Pt fibers which extend through the Nuclepore. Figure 4b shows, as expected, that these fibers assume the shape and dimensions of the host's pores. Furthermore, there are apparently no macroscopic defects in the Pt fibers.

**Evaluation of Capacitance.** As noted in the introduction, it is in principle possible to obtain lower detection limits at UME's than at macro-sized electrodes (1, 2). This detection limit enhancement arises from an improved faradaic current to capacitive current ratio (1, 2). Because of the importance of the capacitive current to the analytical applications of UME's, the double layer capacitances of the UME's were estimated. Cyclic voltammograms were obtained for solutions containing only supporting electrolyte (0.4 M  $\text{Bu}_4\text{ClO}_4$  in MeCN). Typical voltammograms are shown in Figure 5. At

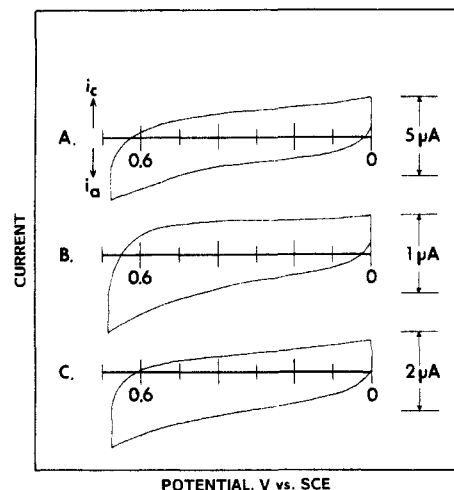


**Figure 5.** Cyclic voltammetry in 0.4 M  $\text{Bu}_4\text{NClO}_4$ , MeCN supporting electrolyte solution: (A) Pt substrate macro-sized electrode,  $A = 0.5 \text{ cm}^2$ ; (B)  $r = 0.5 \text{ } \mu\text{m}$  UME; (C)  $r = 0.1 \text{ } \mu\text{m}$  UME. Scan rate = 100 mV/s.

**Table II.** Comparison of Experimental and Calculated Capacitance Values for UME's

electrode description	$C_d, \mu\text{F}$	
	exptl <sup>a</sup>	calcd <sup>b</sup>
macro, $A = 0.5 \text{ cm}^2$	12	
$r = 0.5 \text{ } \mu\text{m}$ UME	2.75	1.9
$r = 0.1 \text{ } \mu\text{m}$ UME	5.65	1.2

<sup>a</sup> Experimental  $C_d$  = slope of plot of  $i_c$  vs.  $\nu$ . Numbers reflect the average result obtained for three electrodes of each type.

<sup>b</sup> Calculated  $C_d$  values are obtained from the membrane specifications (pore diameter and number density, Table I) by assuming 100% of membrane pores are active elements with a specific capacitance equal to that of the Pt substrate electrode (i.e.  $23.2 \text{ } \mu\text{F cm}^{-2}$ ).

potentials far removed from the switching potential the capacitive current ( $i_c$ ) contribution to the anodic currents shown in Figure 5 are given by (13)

$$i_c = -\nu AC_d \quad (1)$$

where  $\nu$  is the scan rate ( $\text{V s}^{-1}$ ),  $A$  is the electrode area ( $\text{cm}^2$ ), and  $C_d$  is the double-layer capacitance ( $\text{F cm}^{-2}$ ). According to eq 1,  $C_d$  can be obtained from a plot of  $i_c$  vs.  $\nu$ .

Experimental plots of  $i_c$  (at +0.2 V) vs.  $\nu$  are linear for all three electrodes investigated here (correlation coefficients greater than 0.99). Table II compares experimental  $C_d$ 's obtained from these plots with values calculated from the known pore radii and pore densities of the host membranes (see Table I). The calculated values assume that 100% of the pores in the host yield active UME elements with capacitances equal to the capacitance of the bare substrate electrode ( $23.2 \text{ } \mu\text{F cm}^{-2}$ ).

For both UME's, the experimental  $C_d$ 's are larger than the calculated values. Wightman et al. noticed a similar disparity between calculated and experimental  $C_d$ 's and attributed this to defects in the seals between the elements and the host material (14, 15). Because the circumference to area ratio is greater for elements with small radii, problems associated with such defects will be more acute as the radius is decreased (14, 15); this conclusion is in agreement with our data in that the disparity between the calculated and experimental values is greater for the smaller element radius ensembles (Table II).

Capacitance values before incorporation of PE were found to be extremely high, indicating that voids do exist between the Pt elements and the host material. While the molten PE

probably totally fills these voids, PE contracts upon solidification; this contraction undoubtedly opens submicroscopic cracks between the membrane and the elements resulting in increased exposed surface area and higher capacitance values. An insulating material that does not contract upon solidification is required. It is worth noting that we initially used paraffin as an impregnating material but capacitance values were even higher than for the PE-incorporated ensembles. Thus, while PE is a better material, we have obviously not yet found the ideal material.

Obtaining a better sealing material is essential to the analytical applications of these ensembles. Note that if the calculated capacitance could be achieved from the  $0.1\text{-}\mu\text{m}$  UME, an order of magnitude or better decrease in the capacitive current (relative to a macro-sized electrode) would be obtained. This could in principle result in an order of magnitude decrease in detection limits at the UME. Ensembles with even smaller element radii would yield even lower detection limits. However, because of leakage problems for our (and other (14, 15)) UME's, it is pointless to pursue these analytical advantages until a better sealing material is identified. We are currently looking for such a material.

**Evaluation of Faradaic Electrochemical Responses of the UME's.** In addition to providing information about surface area, voltammetric experiments can be used to determine whether the UME's are functioning according to established electrochemical theory (1-3). The shape of the voltammogram obtained at an UME is dependent on the radius of the elements, the distance between adjacent elements, and the time scale (i.e., scan rate) of the experiment (1-3). A qualitative understanding of how these variables effect the voltammogram can be achieved through a consideration of the diffusion layer.

Saveant has suggested that the diffusion layer developed at an UME during a voltammetric experiment can be divided into nonlinear (i.e. radial) and linear diffusion zones (3). If the direction perpendicular to the UME surface is assigned the coordinate  $x$ , the nonlinear diffusion zone extends from  $x = 0$  (i.e., at the UME surface) to a distance  $x = L$ , where  $L$  is approximately equivalent to the distance between the centers of the active sites on the UME surface (3). The linear diffusion zone extends from  $x = L$  to some value  $x = Z$ , where  $Z > L$ . The exact value of  $Z$  depends on the time scale of the experiment; high scan rates yield thin linear diffusion layers (small  $Z$ ) and low scan rates yield thick linear diffusion layers (large  $Z$ ) (3).

The shape of the voltammogram will depend on the relative thicknesses of the nonlinear and linear diffusion zones. Consider the simplest limiting case (2, 3). If the scan rate is very low, the linear diffusion layer will be much thicker than the nonlinear zone and diffusion will be dominated by transport in the thick linear zone. In this case, the voltammogram will look like a conventional semiinfinite linear diffusion voltammogram; indeed, the currents observed will be identical to currents obtained for the same solution at a macro-sized electrode of equivalent geometric area (3). Because capacitive currents are proportional to the small active element area and faradaic currents are proportional to the total geometric area, this limiting case will yield a signal to background advantage and is, therefore, of interest from an analytical point of view (1-3).

As scan rate is increased, the linear diffusion zone becomes thinner. When the scan rate is so high that the linear diffusion layer is much thinner than the nonlinear zone, a second limiting case is reached. In this case, current is dominated by radial diffusion in the nonlinear diffusion zone and the voltammogram assumes a sigmoidal shape (3). As is the case at an ultramicroelectrode (16), current is independent of scan

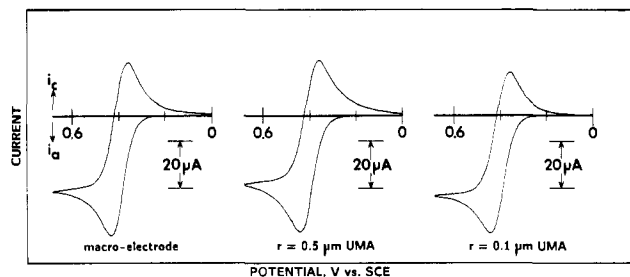


**Figure 6.** Cyclic voltammograms at 5 mV/s in 1 mM ferrocene, 0.4 M  $\text{Bu}_4\text{NClO}_4$ , and acetonitrile for typical  $r = 0.1$  and  $0.5 \mu\text{m}$  UME's and for a macro-sized Pt electrode ( $A = 0.5 \text{ cm}^2$ ).

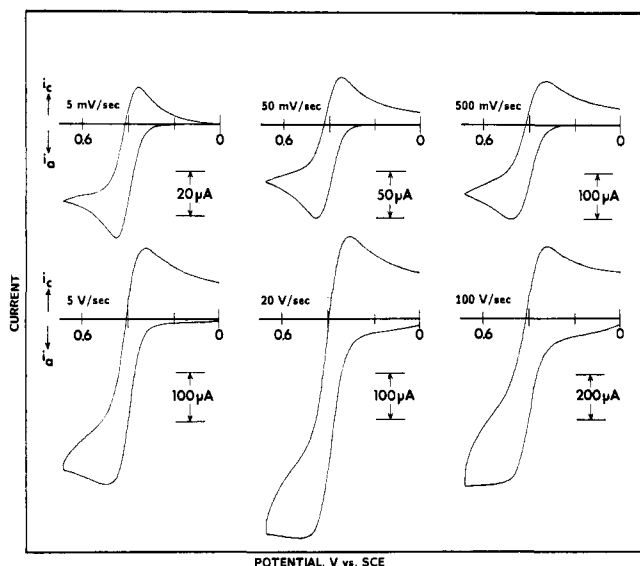


**Figure 7.** Cyclic voltammograms at various scan rates for a typical  $r = 0.5 \mu\text{m}$  UME in 1 mM ferrocene, 0.4 M  $\text{Bu}_4\text{NClO}_4$ , and MeCN. Scan rates are shown.

rate when this limiting case is operative (3). As noted by Wightman, this limiting case can also yield a signal to background advantage (14). Thus, this limiting case is also of interest from an analytical viewpoint.

At even higher scan rates, the nonlinear diffusion zone shrinks, yielding isolated linear diffusion layers at the individual elements of the ensemble (2, 3). The voltammogram again assumes the appearance of a diffusional wave, but the currents are now proportional to only the active area. As we shall see, this limiting case cannot be achieved with the ensembles prepared here. This case does not yield a signal to background enhancement.

Cyclic voltammetric experiments show that the UME's prepared here conform to the theoretical considerations outlined above. Slow scan (5 mV  $\text{s}^{-1}$ ) voltammograms for ferrocene (Fc) are shown in Figure 6. Note that the voltammograms obtained at the UME's are essentially identical to the voltammogram obtained at a macro-sized electrode of the same geometric area. Thus, at this low scan rate, current is dominated by transport in the very thick linear diffusion zone, and the linear diffusion to the total geometric area limiting case, discussed above, is operative. As far as we know, this is the first time that this analytically useful limiting case has been demonstrated experimentally.

Figure 7 demonstrates the effect of scan rate on the shape of the voltammogram at the  $0.5\text{-}\mu\text{m}$  UME. As predicted above, as scan rate increases, the voltammograms begin to acquire a sigmoidal shape. Note, however, that even at the highest scan rate investigated (100 V  $\text{s}^{-1}$ ), the wave still shows a cathodic peak. At higher scan rates, the voltammograms become distorted by uncompensated resistance effects. Thus,

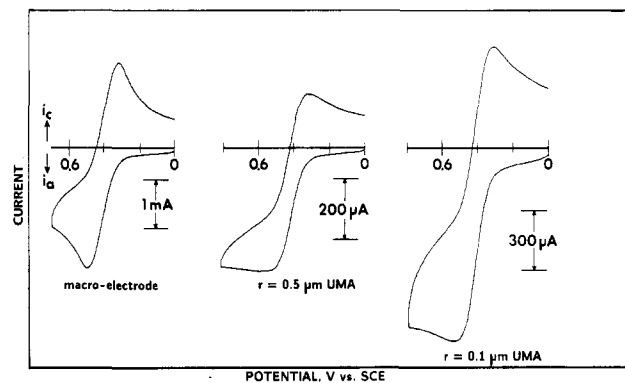


**Figure 8.** Cyclic voltammograms at 20 V/s in 1 mM ferrocene, 0.4 M  $\text{Bu}_4\text{NClO}_4$ , and acetonitrile for typical  $r = 0.1$  and  $0.5 \mu\text{m}$  UME's and a macro-sized Pt electrode ( $A = 0.5 \text{ cm}^2$ ).

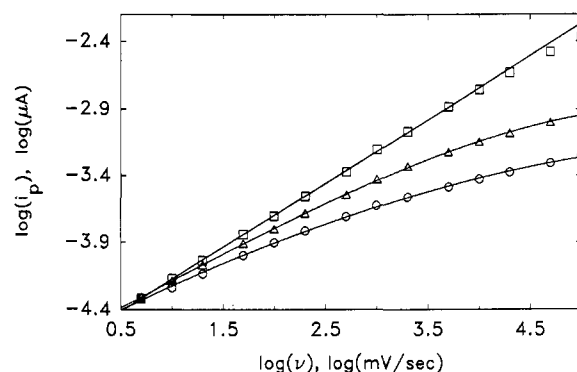


**Figure 9.**  $\log i_p$  vs.  $\log \nu$  for cyclic voltammograms at various electrodes:  $\square$ , macroelectrode;  $\Delta$ ,  $r = 0.1 \mu\text{m}$  UME,  $\circ$ ,  $r = 0.5 \mu\text{m}$  UME. See Figures 6–8 for details.

pure sigmoidal behavior (the second limiting case) could not be achieved with these arrays. The third limiting case, linear diffusion at the individual elements (2, 3), is clearly not possible since this limiting case would require even higher scan rates.

A simple analysis of the relative thicknesses of the linear and nonlinear diffusion zones shows that purely sigmoidal waves would not be expected at the  $0.5\text{-}\mu\text{m}$  UME. As shown in Table I, the average distance between elements in this ensemble is approximately  $5 \mu\text{m}$ . However, electron micrographs indicate that there are many elements which are closer together than this  $5 \mu\text{m}$  average. Thus, the nonlinear diffusion layer will be less than  $5 \mu\text{m}$  in thickness. At  $20 \text{ V s}^{-1}$ , the linear diffusion layer is on the order of  $2 \mu\text{m}$  in thickness (3). Because the linear diffusion layer is still significant compared to the nonlinear layer, a purely sigmoidal wave should not be obtained. The voltammograms in Figure 7 bear out this prediction.

The elements in the  $0.1\text{-}\mu\text{m}$  UME are approximately  $1 \mu\text{m}$  apart (Table I). If the analysis presented above is correct, waves obtained at the  $0.1\text{-}\mu\text{m}$  UME should be even less sigmoidal than voltammograms obtained at the  $0.5\text{-}\mu\text{m}$  UME. Figure 8 compares voltammograms at  $20 \text{ V s}^{-1}$  obtained at the two UME's. Note that as predicted, the  $0.1\text{-}\mu\text{m}$  UME has more pronounced peaks than the  $0.5\text{-}\mu\text{m}$  UME.

Voltammograms such as those shown in Figure 7 may be used to investigate the effect of scan rate ( $\nu$ ) on anodic peak current ( $i_p$ ). Plots of  $\log i_p$  vs.  $\log \nu$  are shown in Figure 9. As would be expected (13), the macroelectrode plot is linear with a slope of 0.5. (Note that peak current begins to fall off at higher scan rates; as indicated above, this is probably caused by uncompensated resistance effects (13).) At very low scan rates, currents for both of the UME's are identical to the current obtained at the macro-sized electrode. This shows that the analytically useful linear diffusion to the total geo-

metric area limiting case can be achieved for both of these ensembles.

As scan rate increases, peak currents at the UME's become significantly less than the macroelectrode values. This diminution in  $i_p$  reflects the transition from the mixed (linear plus radial) diffusion case to the purely radial diffusion case. Note that as would be expected for the purely radial case, the slopes of the plots for the UMA's approach zero at very high scan rates.

If diffusion to the ensemble elements was linear, current would be proportional to the total element area (fractional pore area in Table I), and currents at the 0.5- $\mu\text{m}$  UME would be greater than currents at the 0.1- $\mu\text{m}$  UME. Figure 9 shows that at high scan rates currents at the 0.5- $\mu\text{m}$  UME are, in fact, smaller. This is a manifestation of the transition to the purely radial diffusion limiting case. When this case is operative, the limiting current for the voltammogram is proportional to electrode radius ( $r$ ) rather than electrode area ( $r^2$ ) (16). Thus, the current at each UME will be proportional to the product of the number of elements times the radius of the elements. Because there are many more elements per unit area in the 0.1- $\mu\text{m}$  UME (Table I), the currents at this UME are larger. The data in Figure 9 corroborate the conclusion that, while the purely radial diffusion case cannot be achieved, it can be approximated.

The experiments discussed above show that the electrochemical responses of the UME's prepared here are in qualitative agreement with established theory (1-3). A quantitative evaluation of these UMA's, using a theoretical analysis developed by Pons et al. (17), will be conducted.

### CONCLUSIONS

Because the active electrode area of the 0.1- $\mu\text{m}$  element-radius UME prepared here is 9.4% of the total geometric area (Table I), the total diffusion to the geometric area limiting case should, in principle, yield a signal-to-background ratio enhancement of 9.4, relative to a macro-sized electrode of equivalent geometric area. If this ratio is to be further enhanced, the active area must be decreased. This can be done by incorporating fewer active elements (i.e., by increasing the distance between the elements). This will, however, make it more difficult to achieve the linear diffusion to the total geometric area limiting case.

This problem can be circumvented by making the elements smaller and, thereby, increasing the radial contributions to diffusion at each element. Thus, if the electroanalytical advantages of UMA's are to be realized, devices with smaller and fewer elements must be prepared. We are currently working toward this goal.

In the most general sense, we describe in this paper a procedure for preparing uniformly sized and shaped metallic (or other material) microstructures. Such microstructures might be useful in a variety of chemical applications. For example, we have recently shown that electronically conductive polymer membranes having microfibrous morphologies can be prepared using the methods described in this paper (11). These microfibrous membranes support higher rates of ion transport than conventional, amorphous electronically conductive polymer membranes (18). This has important im-

plications for battery and other electronic applications of these polymers (11, 18).

Furthermore, note that Figure 4b suggests that the procedures developed here might be useful for dispersing very small, uniformly sized and shaped metallic particles onto conductive surfaces. It seems possible that unique catalyst structures could be prepared by using this approach. For example, the semiconductor electrode surface in a photoelectrochemical cell is often coated with small metal catalyst particles (19-21). Since the method described here offers the possibility of precisely controlling the size, shape, and density of the metal microparticles produced, this procedure could prove useful in such photoelectrochemical experiments. Fuel cell and other catalyst particles might also be prepared by using this approach.

We are currently investigating a number of these possibilities. For example, we have recently shown that Pt microcylinders like those shown in Figure 4b can be photoelectrochemically grown on silicon surfaces (22). We will report the results of these and related studies in future papers.

### ACKNOWLEDGMENT

The authors acknowledge Stan Pons for valuable consultation and Nuclepore Corporation for donating the Nuclepore membranes. This work was supported by the Office of Naval Research, the Robert A. Welch Foundation, and the Dow Chemical Co.

Registry No. Pt, 7440-06-4.

### LITERATURE CITED

- (1) Reller, H.; Kirowa-Eisner, E.; Gileadi, E. *J. Electroanal. Chem. Interfacial Electrochem.* **1984**, *161*, 247.
- (2) Cassidy, J.; Ghoroghchian, J.; Sarfarazi, F.; Smith, J. J.; Pons, S. *Electrochim. Acta* **1986**, *31*, 629.
- (3) Amatore, C.; Saveant, J. M.; Tessier, D. J. *Electroanal. Chem. Interfacial Electrochem.* **1983**, *147*, 39.
- (4) Hefel, T.; Osteryoung, J. J. *Electrochem. Soc.* **1986**, *133*, 752.
- (5) Broers, A. N. J. *Electrochem. Soc.* **1981**, *128*, 166.
- (6) Broers, A. N.; Harper, J. M. E.; Molzen, W. W. *Appl. Phys. Lett.* **1978**, *33*, 392.
- (7) Flanders, D. C. *Appl. Phys. Lett.* **1980**, *36*, 93.
- (8) Product literature on Nuclepore polycarbonate membranes, Nuclepore Corp., Pleasant, CA.
- (9) Roe, David K. In *Laboratory Techniques in Electroanalytical Chemistry*; Kissinger, P. T., Heineman, W. R. Eds.; Marcel Dekker: New York, 1984; Chapter 7.
- (10) Penner, R. M.; Martin, C. R. *J. Electrochem. Soc.* **1986**, *133*, 310.
- (11) Penner, R. M.; Martin, C. R. *J. Electrochem. Soc.* **1986**, *133*, 2206.
- (12) Penner, R. M., unpublished work, Texas A&M University, Feb 1987.
- (13) Bard, Allen J.; Faulkner, Larry R. *Electrochemical Methods: Fundamentals and Applications*; Wiley: New York, 1980; Chapter 1 and 6.
- (14) Wehmeyer, K. R.; Deakin, M. R.; Wightman, R. M. *Anal. Chem.* **1985**, *57*, 1913.
- (15) Wehmeyer, K. R.; Wightman, R. M. *J. Electroanal. Chem. Interfacial Electrochem.* **1985**, *196*, 417.
- (16) Wightman, R. M. *Anal. Chem.* **1985**, *53*, 1125A.
- (17) Pons, S., unpublished work, University of Utah, Dec 1986.
- (18) Penner, R. M.; Martin, C. R.; Presented at the 193rd National Meeting of the American Chemical Society, Denver, CO, April 7, 1987.
- (19) Heller, A.; Aspnes, D. E.; Porter, J. D.; Sheng, T. T.; Vadimsky, R. G. *J. Phys. Chem.* **1985**, *89*, 4444.
- (20) Heller, A.; Aharon-Shalom, E.; Bonner, W. A.; Miller, B. J. *Am. Chem. Soc.* **1982**, *104*, 6942.
- (21) Nakato, Y.; Kelichi, U.; Tsubomura, H. *J. Phys. Chem.* **1986**, *90*, 5495.
- (22) Penner, R. M., unpublished work, Texas A&M University, Dec 1986.

RECEIVED for review March 30, 1987. Accepted June 26, 1987.